A Reconfigurable Graphene Patch Antenna Inverse Design at Terahertz Frequencies

Mohammad Mashayekhi
Iran University of Science and Technology
Pooria Kabiri
Iran University of Science and Technology
Amir saman Nooramin (a_nooramin@iust.ac.ir)
Iran University of Science and Technology
Mohammad Soleimani
Iran University of Science and Technology

Article

Keywords:

Posted Date: February 6th, 2023

DOI: https://doi.org/10.21203/rs.3.rs-2511137/v1

Additional Declarations: No competing interests reported.

Version of Record: A version of this preprint was published at Scientific Reports on May 24th, 2023. See the published version at https://doi.org/10.1038/s41598-023-35036-4.

A Reconfigurable Graphene Patch Antenna Inverse Design at Terahertz Frequencies

Mohammad Mashayekhi[1], Pooria Kabiri[1], Amir saman Nooramin[1,*], and Mohammad Soleimani[1]

[1]Iran University of Science and Technology,School of Electrical Engineering, Tehran, 1684613114, Iran
[*]a_nooramin@iust.ac.ir

ABSTRACT

This article investigates the inverse design of a reconfigurable multi-band patch antenna based on graphene for terahertz applications to operate frequency range (2THz – 5THz). In the first step, this article evaluates the dependence of the antenna radiation characteristics on its geometric parameters and the graphene properties. The simulation results show that it is possible to achieve up to 8.8 dB gain, 13 frequency bands, and 360° beam steering. Then and due to the complexity of the design of graphene antenna, a deep neural network (DNN) is used to predict the antenna parameters by given inputs like desired realized gain, main lobe direction, half power beam width, and return loss in each resonance frequency. The trained DNN model predicts almost with 93% accuracy and 3% mean square error in the shortest time. Then, this network was used to design five-band and three-band antennas, and it has been shown that the desired antenna parameters are achieved with negligible errors. Therefore, the proposed antenna finds many potential applications in the THz frequency band.

Introduction

Nowadays, the terahertz band is used in wireless telecommunications[1], hyperthermia treatment of breast cancer[2], biomedical imaging, security screening, and material identification[3] due to its remarkable properties. In wireless communication, the need for multi-band antennas has increased due to a reduction in the number of antennas, a reduction in the complexity and cost of the system, and providing the possibility of integration with other circuits of the structure[4,5].

On the other hand, the use of graphene has been very impressive in recent years in the field of Nano-electronic and THz devices due to its high conductivity and the changeability of the conductivity by tuning the bias voltage. The use of graphene in THz imaging[6], patch antennas[7–9] ultra-broadband absorbers[10], and photoconductive antennas[11] has been reported. In[12], a dual-band antenna with an average gain of 2.45 dB is designed by creating two circle strips on the graphene. In[13], a three-band frequency reconfigurable antenna has been proposed for a slotted patch graphene antenna. In[14], a three-band antenna is implemented with a series feed circle graphene patch with a gain close to 10 dB. In[15], a four-band antenna has been reported for a four L-shaped stub graphene patch antenna. Generally, for graphene antennas, it is possible to change the number of operating frequency bands by the variation of graphene chemical potential, similar to[16,17] in which a four-band and three-band graphene antenna has been designed with the gain of 2.58 dB and 9.51 dB, respectively.

Making less computational time of resources with an acceptable result is of substantial importance in electromagnetic applications. In this regard, the machine learning approach has recently demonstrated outstanding performance compared to the computational and iterative methods in dealing with electromagnetic problems. Deep learning (DL) or DNN is a subset of machine learning (ML) with more robust computing capabilities, which is based on neural networks (NNs) and can learn the nexus between inputs and outputs. After learning, the designed model based on trained data can show a reasonable prediction as outputs for various given inputs in a fraction of a second. By taking advantage of this, DL was a suitable technique for inverse scattering problems[18,19], metasurface design[20,21], beamforming[22,23], design of antenna[24–26].

We have classified using the neural networks in antenna design into three approaches. First, NNs and ML enhance some radiation properties by optimizing the antenna parameters and can not control antenna radiation patterns in real-time[27]. Second, by giving the antenna dimensions as input, the antenna radiation will be estimated as output in real-time so DL and ML can speed up the antenna simulation directly[24,25]. And third, the most widely used method is the inverse design of the antenna using DL. The required radiation pattern characteristics are provided as input, and the DNN's output estimates the antenna parameters. In this case, depending on the circumstances, the antenna parameters may be fully adjustable or non-adjustable[22,26]. Although in[23] a VO_2 is used as a reconfigurable component in the antenna, the proposed DNN outputs geometrical antenna parameters.

In this article, an inverse design of reconfigurable graphene circular patch antenna at THz frequencies is proposed and surveyed to the realization of an intelligent antenna for 6G wireless communication. Also, for the first time we apply a chemical

potential of graphene as a reconfigurable component in the output of DNN to control the radiation properties in real-time. The antenna parameters are divided into two groups, variable and constant parameters. After analysis we generate data set with variable parameters then filter data set with two conditions. Then, a deep neural network is presented, which can accurately estimate the values of the structural parameters of the antenna for desired the number of frequency bands and the main lobe directions. So we could control the radiation parameters of the graphene antenna with reconfigurable parameters of graphene and antenna geometry.

For this, in section II, the design and simulation of the antenna have been discussed. Then, the used deep learning method will be explained and the achieved results have been examined in section III. Finally, some conclusions are remarked.

1 Antenna Design and Simulation

The flow chart of the activity steps is plotted in Fig. 1. At first, the behavior and dependency of the antenna characteristics on its parameters are investigated by taking into account the antenna parameters are divided into two groups, variable and constant parameters (see Fig. 1 (a)). Secondly, the data needed for training the DNN model is generated by changing variable parameters in antenna simulations (see Fig. 1(b)). Thirdly, after coding and excerpting the data, we organized it to achieve better performance for the DNN model (see Fig. 1(c)). Finally, we present a DNN model, which can accurately estimate the values of the thickness of the substrate, τ, and μ_c for desired inputs. In this work, Desired inputs of DNN comprise resonance frequencies, realized gain, null level, main lobe direction, and half-power beam width (see Fig. 1(d)). Based on the mentioned procedure, each section will be explained below.

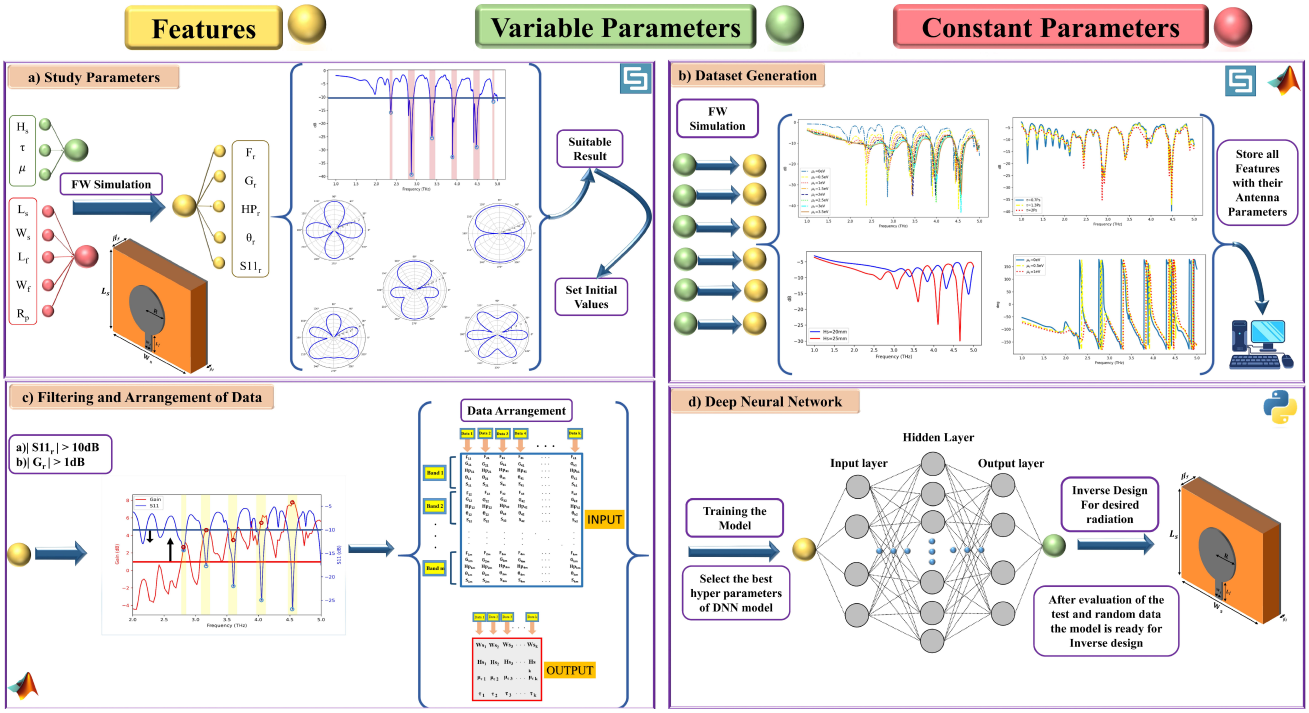

Figure 1. flow chart of the main steps in the inverse design of graphene patch antenna

1.1 Antenna structure definition

The structure of the antenna along with its parameters is plotted in Fig. 2. As shown in this figure, the structure is comprised of three layers. At the top and bottom, a graphene layer with thickness $H_g = 0.08$mm and temperature $T_k = 273$K is deposited. For the middle layer, a silicon layer by the relative permeability $\varepsilon_r = 11.9$ and conductivity $\sigma = (25 * 10^{-5})$ is used. The other characteristics and dimensions of layers are given in table. 1. A 50-ohm microstrip feed line is used in this structure, as shown in Fig. 1. After the explanation of the antenna structure, the influence of parameters on the radiation characteristics is explained in the next section.

1.2 Antenna parameter study and the generation of data sets

In this section, the effect of antenna parameters on the radiation properties is studied and the results are categorized to learn the neural network. For this, full-wave simulations are done in CST Microwave Studio. The study parameters include chemical

Parameters	Range
μ_c	[0-2] eV
τ	[0.1-1] ps
H_s	[10-30] μm
W_s and L_s	[50-90] μm
R_p	[15-25] μm
H_g	[0.01-0.1] μm
W_f	[4-12] μm
L_f	[8-20] μm

Table 1. Range of initial values of the antenna parameters

potential (μ_c = [0-7] eV), relaxation time (τ = [0.1-2] ps), substrate thickness (H_s = [20,30] μm), the width of the substrate (W_s = [70,90] μm), the patch radius (R_p = [18,25] μm), the feed length (L_f = 17 μm), the feed width (W_f = 6 μm), and the graphene thickness (H_g = 0.08 μm) . Finally, the number of simulations is equal to 2880. It is worth mentioning that the simulations are done in the frequency range of [1-5] THz and S_{11}, radiation pattern in E-plane, and realized gain is extracted in 101 equally spaced frequency points in the mentioned bandwidth. Then, the number and directions of main beams are extracted from the realized gain data based on the condition $G_{realized} > 1$dB. Furthermore, the number of frequency bands is determined on the condition that $|S_{11}| > 10$dB. In the next step, the dependency of the antenna characteristics on the parameter values will be investigated.

1.3 Studying the dependence of antenna characteristics on the values of its parameters

In Figs. 3 (a) and (b), the number of frequency bands is studied as a function of the relaxation time and the chemical potential for H_s = 20 μm and H_s = 30 μm, respectively. As shown in this figure, the number of frequency bands enhances with increasing chemical potential. Also, the antenna with a thicker substrate will create more frequency bands. Furthermore, Changing the relaxation time will not affect the increase in the number of frequency bands for the zero chemical potential. It is worth mentioning that in Fig. 3, the color bar is devoted to relaxation time to make more clearance. Similarly, in Figs. 3 (c) and (d) the center of the frequency bands which is named here as the resonance frequency, has been studied. As shown in this figure, multi-band operation is achieved for lower values of relaxation time chemical potential. Likewise, high values of chemical potential and relaxation time will result in higher frequency bands. Resonance frequencies in the range of [2-3] THz are achieved if H_s=30 μm. In the same manner, Figs. 3 (e) and (f) are devoted to studying gain. As shown in these figures, the values of gain are distributed in the range of [1-8.8]dB. Furthermore, higher gain values are achieved for thicker substrates and lower chemical potentials. In Figs. 3 (g) and (h), the angles of the main lobe directions are plotted. Based on the presented results in this figure, the distribution of the main lobe angle is wider for higher values of relaxation time, chemical potentials, and substrate thickness and can cover all the range of [0-360] degrees.

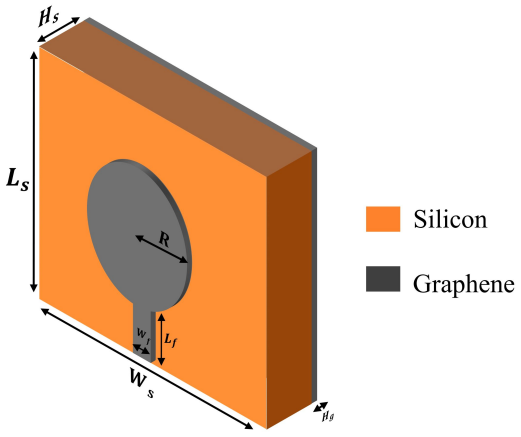

Figure 2. The structure of the patch antenna

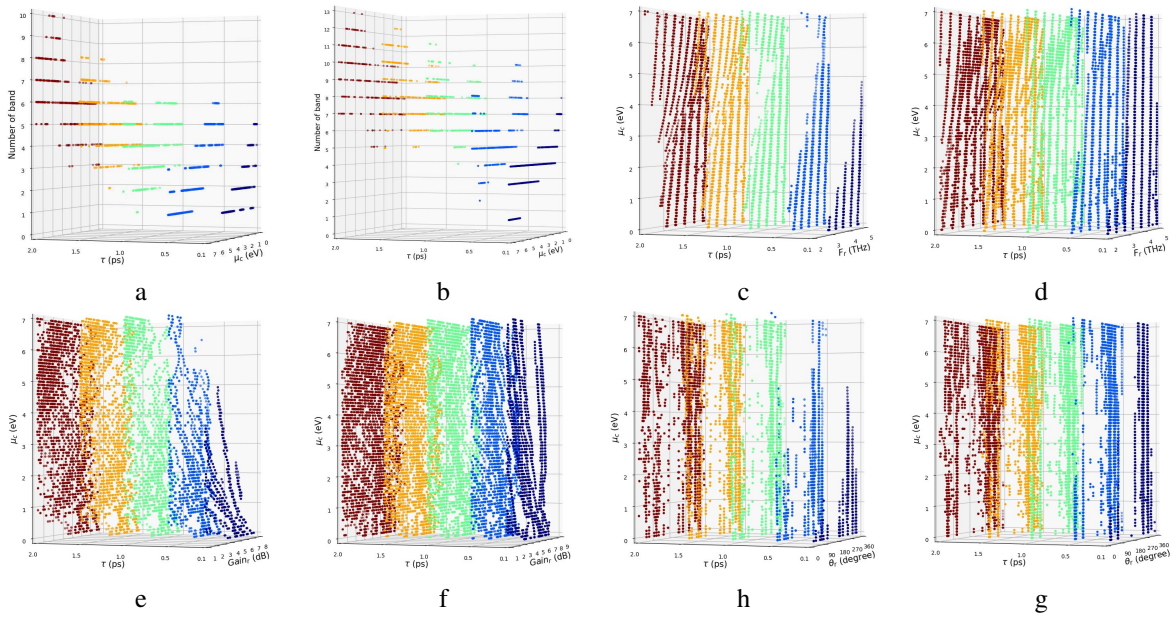

Figure 3. the study of the radiation properties of the antenna as a function of relaxation time (τ), and chemical potential (μ_c). antenna. The number of frequency bands (a,b), resonance frequency [THz] (c,d), gain [dB] (e,f), and main beam direction [degree] (g, h).

2 Deep learning

Artificial neural networks are machine learning techniques inspired by the human nervous system. The neural network consists of interconnected neurons, and by changing the weight of the interconnected neurons, they can learn the input and output relationship and generalize it based on empirical knowledge. Fig. 4 shows the schematic of a neural network. In this figure, n is the number of inputs and x_i is the value of each input. Each input has a specific weight called w_i, which is multiplied by the input and added. After summation, an activation function (ϕ) is provided to estimate the output, which can be biased with an initial value (b). In equation (1), the output and input of the neural network are presented. Neural networks include an input layer, one/several hidden layers, and an output layer, and each layer has a specific number of neurons. Also, the weights of each neuron will change during a back propagation process to learn the input and output relationship pattern. In general, as the number of neurons and hidden layers increases, the ANN network becomes more DNN, which will cause the complexity of the model.

$$Y = \phi\left(\sum_{i=1}^{n} W_i X_i + b_i\right) \tag{1}$$

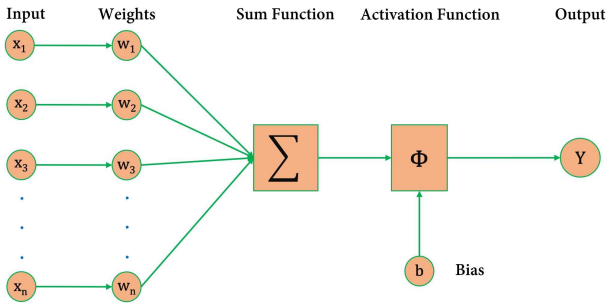

Figure 4. Schematic of neural network

In this research, the inputs of the deep neural network include the number of bands, the resonance frequencies of the bands, the beam direction, the half-power beam width, the gain, and the depth value of S_{11} at each resonance frequency of the antenna. After the presented neural network has been learned, the required antenna parameters including the dimensions of the antenna

and the characteristics of the required graphene can be estimated. As mentioned later, the maximum number of bands is assumed to be m=13. Therefore, each input vector is a row matrix of order 65 including the vector for each 13 frequency bands. In the proposed learning procedure, 60% of data has been used for learning while the others are used in the test sequence.

The output of the neural network includes a third-order vector including the thickness of the substrate, relaxation time, and chemical potential. Since the goal of this research is to accurately estimate the antenna parameters, thus the Relu activation function has been used in each network layer. It should be noted that the number of layers and neurons was optimized to achieve the best performance in the proposed network. In the proposed model, the batch size and learning rate are 512 and 0.001, respectively, and the epoch number is equal to 5000. Also, Adam's powerful optimization algorithm has been used to determine the values of the weights in the model. Furthermore, the utility cost function MSE has been used to calculate the difference between the real value and the value estimated by the model, which is given in equation 2 whereas y_i and f_i are real and estimated values, respectively.

$$MSE = \frac{1}{N}\sum_{i=1}^{N}(f_i - y_i)^2 \tag{2}$$

To achieve the best performance of DNN, we had several tests on the combination of layers and their output shape value. Table 2 shows the best structure of DNN for learning the relationship between inputs and outputs.

Layers	Activation	Output Shape	Parameters Number
Dense	Relu	(None,65)	4290
Dense	Relu	(None,200)	13200
Dropout	-	(None,200)	0
Dense	Relu	(None,200)	40200
Dropout	-	(None,200)	0
Dense	Relu	(None,200)	40200
Dropout	-	(None,200)	0
Dense	Relu	(None,3)	603

Table 2. The configuration of proposed DNN model

The loss and accuracy diagrams of the proposed model have been sketched in Figs. 5(a) and (b), respectively. As can be seen in this figure, the values of accuracy and loss achieve 91.5% and 0.03, respectively. Furthermore, it can be seen that the validation graph is very close to the training graph and was able to avoid overfitting in the model. In this procedure, the training time was about 262 seconds and the model can estimate the output in less than 0.05 seconds which was obtained in a system with an Intel Core i7-10750H processor and 16GB RAM.

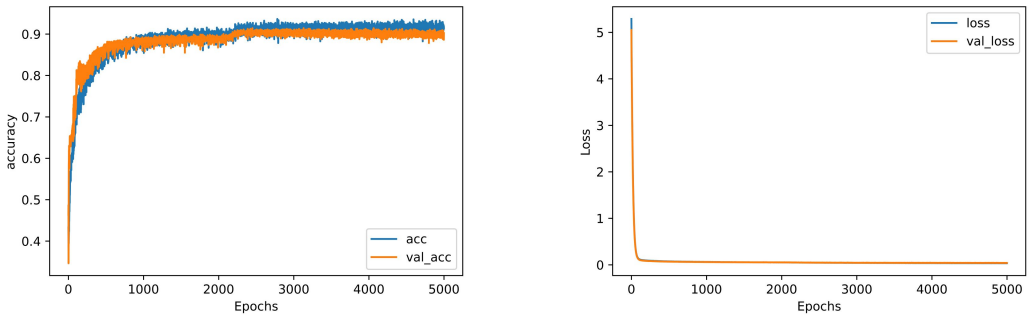

(a) (b)

Figure 5. (a) accuracy and (b) loss of the proposed DNN.

3 Evaluation of deep neural network

For the evaluation of the proposed model, we have provided two arbitrary samples whose specifications are given in Figure 6. For this, the desired values are fed to the proposed network and the antenna parameters are estimated. Then, a full wave

analysis has been done to simulate the performance of the antenna. As shown in Figs. 6(a) and (b), the gain and return loss of a five-band and a three-band antenna are plotted versus frequency, respectively. In these figures, the desired values are also shown using colored circles and are in good agreement with the simulation results. In the same way, the simulation results and the desired values of the half-power beam width and the main lobe direction for five-band and three-band antennas are plotted in Figs. 6(c) and (d), respectively. The small differences between the simulated and expected values are also evident in these figures. The estimated values of the substrate thickness, chemical potential, and relaxation time are presented in Table 3. Furthermore, the Mean Square Error of the resonance frequencies, half-power beam width, gain and return loss are shown in table 3. According to these results, it can be claimed that a negligible error in the antenna desired parameters will be obtained by the estimation of antenna thickness and graphene properties.

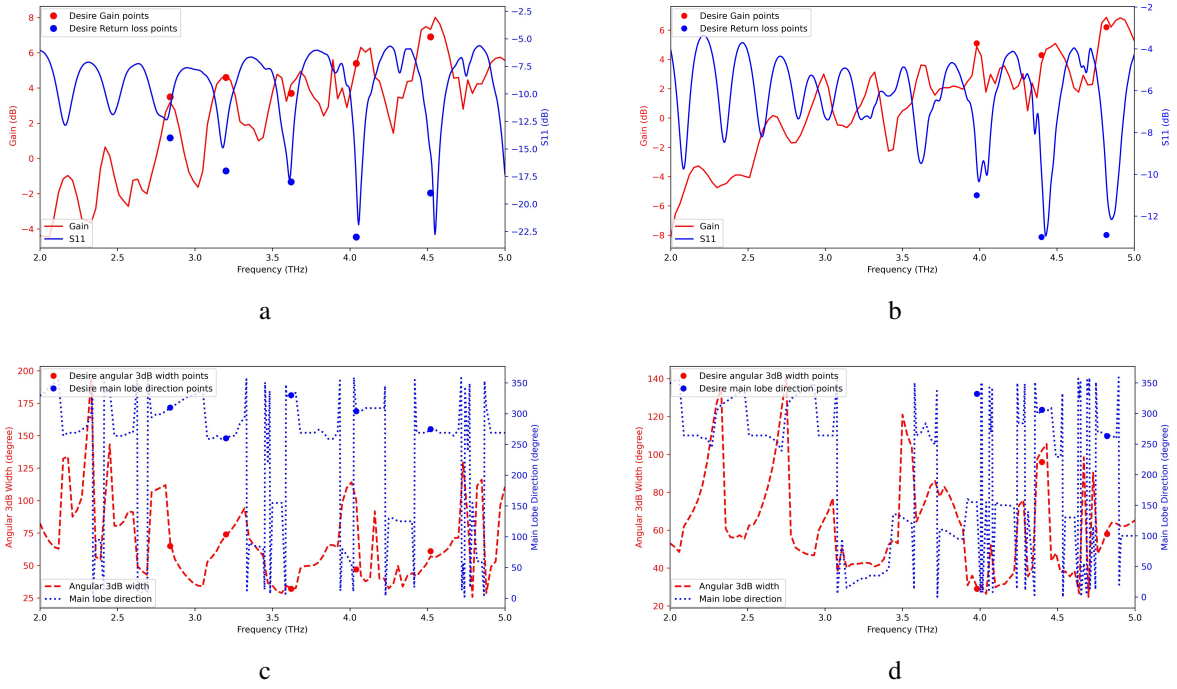

Figure 6. (a) and (b) simulation and expected values gain and S_{11} for a five-band and three-band antenna, respectively. (c) and (d) simulation and expected values of half-power beam width and main lobe direction for five-band and three-band antenna, respectively. In this figure, expected values have been specified by colored circles.

	Estimated outputs			MSE between f_i and y_i				
Examples	H_s	τ	μ_c	F_r	G_r	θ_r	HP_r	$Null_r$
Five-band	30 μm	0.50 ps	3.13 eV	$1.2e^{-5}$	$1.92e^{-3}$	$1.69e^{-5}$	$2.3e^{-4}$	$25e^{-4}$
Three-band	20 μm	0.94 ps	2.64 eV	$4e^{-5}$	$25.7e^{-3}$	$3.59e^{-5}$	$6e^{-4}$	$2e^{-4}$

Table 3. Estimated values and Mean Square Error (MSE) of predicted and real antenna properties. performance

Discussion

In this article, a planar graphene antenna was investigated and its radiation characteristics for different substrate thicknesses and graphene characteristics including chemical potential and relaxation time have been extracted by full-wave FEM simulations. Then, these parameters were examined as the design inputs and it was shown that in the proposed structure, by choosing the appropriate values for the input, the number of bands and their resonance frequencies, antenna gain and main lobe directions can be set. The simulations have been performed in the [2-5] THz frequency band and it has been shown that the maximum gain of 8.8dB and up to 13 frequency bands can be achieved. Due to the complexity of the design and in the following, a deep neural network has been used to provide a design solution. This network is trained based on the categorized simulation results and the network parameters are determined in such a way that the most accurate matching between the estimated and simulated

parameters has been achieved for minimum input data. In the end, it has been shown that the optimal radiation parameters can be estimated with an error of less than 3%. This feature can be used to design antennas in various applications.

References

1. Rappaport, T. S. *et al.* Wireless communications and applications above 100 GHz: Opportunities and challenges for 6g and beyond. *IEEE Access* **7**, 78729–78757, DOI: 10.1109/ACCESS.2019.2921522 (2019).
2. Mahmoud, K. R. & Montaser, A. M. Design of Multi-Resonance Flexible Antenna Array Applicator for Breast Cancer Hyperthermia Treatment. *IEEE Access* **PP**, 1–1, DOI: 10.1109/access.2022.3203431 (2022).
3. Malhotra, I., Jha, K. R. & Singh, G. Terahertz antenna technology for imaging applications: A technical review. *Int. J. Microw. Wirel. Technol.* **10**, 271–290, DOI: 10.1017/S175907871800003X (2018).
4. Mahabub, A., Rahman, M. M., Al-Amin, M., Rahman, M. S. & Rana, M. M. Design of a Multiband Patch Antenna for 5G Communication Systems. *Open J. Antennas Propag.* **06**, 1–14, DOI: 10.4236/ojapr.2018.61001 (2018).
5. Maci, S. & Biffi Gentili, G. Dual-frequency patch antennas. *IEEE Antennas Propag. Mag.* **39**, 13–19, DOI: 10.1109/74.646798 (1997).
6. Hosseininejad, S. E. *et al.* Reprogrammable graphene-based metasurface mirror with adaptive focal point for thz imaging. *Sci. Reports* **9** (2019).
7. Alibakhshikenari, M. *et al.* High-isolation antenna array using SIW and realized with a graphene layer for sub-terahertz wireless applications. *Sci. Reports* **11**, 1–14, DOI: 10.1038/s41598-021-87712-y (2021).
8. Khan, M. A. K., Ullah, M. I., Kabir, R. & Alim, M. A. High-Performance Graphene Patch Antenna with Superstrate Cover for Terahertz Band Application. *Plasmonics* **15**, 1719–1727, DOI: 10.1007/s11468-020-01200-z (2020).
9. Shamim, S. M., Das, S., Hossain, M. A. & Madhav, B. T. P. Investigations on Graphene-Based Ultra-Wideband (UWB) Microstrip Patch Antennas for Terahertz (THz) Applications. *Plasmonics* **16**, 1623–1631, DOI: 10.1007/s11468-021-01423-8 (2021).
10. Liu, L., Liu, W. & Song, Z. Ultra-broadband terahertz absorber based on a multilayer graphene metamaterial. *J. Appl. Phys.* **128**, DOI: 10.1063/5.0019902 (2020).
11. Nissiyah, G. J. & Madhan, M. G. Graphene-Based Photoconductive Antenna Structures for Directional Terahertz Emission. *Plasmonics* **14**, 891–900, DOI: 10.1007/s11468-018-0871-7 (2019).
12. Nickpay, M. R., Danaie, M. & Shahzadi, A. Wideband Rectangular Double-Ring Nanoribbon Graphene-Based Antenna for Terahertz Communications. *IETE J. Res.* **68**, 1625–1634, DOI: 10.1080/03772063.2019.1661801 (2022).
13. M, S. & M, G. M. Performance predictions of slotted graphene patch antenna for multi-band operation in terahertz regime. *Optik* **204**, 164223, DOI: 10.1016/j.ijleo.2020.164223 (2020).
14. Vijayalakshmi, K., Selvi, C. S. & Sapna, B. Novel tri-band series fed microstrip antenna array for THz MIMO communications. *Opt. Quantum Electron.* **53**, 1–13, DOI: 10.1007/s11082-021-03065-w (2021).
15. Bokhari, B. S. M., Bhagyaveni, M. A. & Rajkumar, R. On the use of graphene for quad-band THz microstrip antenna array with diversity reception for biomedical applications. *Appl. Phys. A: Mater. Sci. Process.* **127**, 1–9, DOI: 10.1007/s00339-021-04616-4 (2021).
16. Nissiyah., G. J. & Madhan, M. G. Graphene based microstrip antenna for triple and quad band operation at terahertz frequencies. *Optik* **231**, 166360 (2021).
17. Kavitha, S., Sairam, K. V. & Singh, A. Graphene plasmonic nano-antenna for terahertz communication. *SN Appl. Sci.* **4**, DOI: 10.1007/s42452-022-04986-1 (2022).
18. Wei, Z. & Chen, X. Deep-Learning Schemes for Full-Wave Nonlinear Inverse Scattering Problems. *IEEE Transactions on Geosci. Remote. Sens.* **57**, 1849–1860, DOI: 10.1109/TGRS.2018.2869221 (2019).
19. Li, Y. *et al.* Predicting Scattering from Complex Nano-Structures via Deep Learning. *IEEE Access* **8**, 139983–139993, DOI: 10.1109/ACCESS.2020.3012132 (2020).
20. An, S. *et al.* Deep learning modeling approach for metasurfaces with high degrees of freedom. *Opt. Express* **28**, 31932–31942, DOI: 10.1364/OE.401960 (2020).
21. Ghorbani, F. *et al.* Deep neural network-based automatic metasurface design with a wide frequency range. *Sci. Reports* **11**, 1–8, DOI: 10.1038/s41598-021-86588-2 (2021). 2101.10866.

22. Tan, Y. J. *et al.* Self-adaptive deep reinforcement learning for THz beamforming with silicon metasurfaces in 6G communications. *Opt. Express* **30**, 27763, DOI: 10.1364/oe.458823 (2022).

23. Dao, R.-N. *et al.* The reverse design of a tunable terahertz metasurface antenna based on a deep neural network. *Microw. Opt. Technol. Lett.* **65**, 264–272, DOI: https://doi.org/10.1002/mop.33471 (2023). https://onlinelibrary.wiley.com/doi/pdf/10.1002/mop.33471.

24. Shi, L. P., Zhang, Q. H., Zhang, S. H., Yi, C. & Liu, G. X. Efficient Graphene Reconfigurable Reflectarray Antenna Electromagnetic Response Prediction Using Deep Learning. *IEEE Access* **9**, 22671–22678, DOI: 10.1109/ACCESS.2021.3054944 (2021).

25. Stankovic, Z. Z., Olcan, D. I., Doncov, N. S. & Kolundzija, B. M. Consensus Deep Neural Networks for Antenna Design and Optimization. *IEEE Transactions on Antennas Propag.* **70**, 5015–5023, DOI: 10.1109/TAP.2021.3138220 (2022).

26. Sharma, K. & Pandey, G. P. Efficient modelling of compact microstrip antenna using machine learning. *AEU - Int. J. Electron. Commun.* **135**, 153739, DOI: 10.1016/j.aeue.2021.153739 (2021).

27. Shi, D., Lian, C., Cui, K., Chen, Y. & Liu, X. An Intelligent Antenna Synthesis Method Based on Machine Learning. *IEEE Transactions on Antennas Propag.* **70**, 4965–4976, DOI: 10.1109/TAP.2022.3182693 (2022).

Author contributions statement

M.M. and P.K. conceived the idea. M.M. set up the DNN model. P.K. designed and analyzed the graphene antenna. Finally, A.N. wrote the manuscript based on the input from all authors and A.N. and M.S. supervised the project and reviewed the manuscript.

Competing interests

The authors declare no competing interests.

Additional information

Correspondence and requests for materials should be addressed to A.N.

Data availability: The data that support the findings of this study are available from A.N. but restrictions apply to the availability of these data, which were used under license for the current study, and so are not publicly available. Data are however available from the authors upon reasonable request and with permission of A.N. (email: a_nooramin@iust.ac.ir).